Nonlinear dynamics of a two-level system of a single spin driven beyond the rotating-wave approximation

K. Rama Koteswara Rao and Dieter Suter
Fakultät Physik, Technische Universität Dortmund, D-44221 Dortmund, Germany
(Received 17 October 2016; published 1 May 2017)

Quantum systems driven by strong oscillating fields are the source of many interesting physical phenomena. In this work, we experimentally study the dynamics of a two-level system of a single spin driven in the strong-driving regime where the rotating-wave approximation is not valid. This two-level system is a subsystem of a single nitrogen-vacancy (NV) center in diamond coupled to a first-shell ^{13}C nuclear spin at a level anticrossing point. This near degeneracy occurs in the $m_s = \pm 1$ manifold of the electron spin when the energy level splitting between the $m_s = -1$ and $+1$ states due to the static magnetic field is $\approx$127 MHz and thus equal to the splitting due to the ^{13}C hyperfine interaction. The transition frequency of this electron spin two-level system in a static magnetic field of 28.9 G is 1.7 MHz and it can be driven only by the component of the radio-frequency (RF) field along the NV symmetry axis. Electron spin Rabi frequencies in this system can reach tens of MHz even for moderate RF powers. The simple sinusoidal Rabi oscillations that occur when the amplitude of the driving field is small compared to the transition frequency evolve into complex patterns when the driving field amplitude is comparable to or greater than the energy level splitting. We observe that the system oscillates faster than the amplitude of the driving field and the response of the system shows multiple frequencies.

DOI: 10.1103/PhysRevA.95.053804

I. INTRODUCTION

Two-level systems are the basis for many important fundamental concepts in diverse areas of physics, including various types of resonance phenomena [1,2]. A quantum bit or qubit, which is realized physically by a two-level quantum system, is the fundamental building block of quantum computation and quantum information protocols [3].

A two-level system is equivalent to a spin-$\frac{1}{2}$ particle precessing in a static magnetic field, where the spin precession frequency is equal to the frequency separation between the two levels. Resonance occurs when an oscillating field with a frequency equal to the spin precession frequency is applied in a direction perpendicular to the static field. In most experimental situations, the driving field is a linearly oscillating one and it can be written as a sum of a co- and a counter-rotating field with respect to the spin precession. Most of the fundamental concepts in optical and magnetic resonance are derived in the so-called weak-driving regime, where the amplitude of the driving field is much smaller than the spin precession frequency. In this regime, the effect of the counter-rotating field component can be neglected, which is known as the rotating-wave approximation [2]. The corotating field component causes harmonic oscillations between the two levels, which are known as Rabi oscillations. In the strong-driving regime, where the amplitude of the driving field is of the order or greater than the spin precession frequency, the rotating-wave approximation breaks down and the counter-rotating field component, which cannot be neglected anymore, leads to many interesting physical phenomena [4–7]. In this regime, the system's dynamics are highly anharmonic and nonlinear, but not chaotic [8,9]. Recently, the strong-driving regime has been of particular interest to quantum information processing because of the ultrafast quantum gates possible in this regime [10–15].

In this work, we experimentally observe the anharmonic and nonlinear dynamics of a two-level system of a single solid-state spin driven in the strong-driving regime. The system of interest is a single nitrogen-vacancy (NV) center (electron spin $S = 1$) in diamond coupled to a first-shell ^{13}C nuclear spin ($I = 1/2$) and the intrinsic ^{14}N nuclear spin ($I = 1$) of the center, which together form an 18-level system. A small static magnetic field is applied at an orientation such that the energy level splitting due to the Zeeman interaction of the electron spin is equal to the corresponding splitting due to the ^{13}C hyperfine interaction, which is approximately 127 MHz. At this point, level anticrossings (LACs) occur between the $m_s = -1$ and $+1$ spin sublevels due to the strong nonsecular components of the Hamiltonian. Far away from the LAC, electron spin transitions between these spin-sublevels are forbidden. At the LAC point, the $m_s = +1$ and -1 spin states are completely mixed and a transition can be excited between these levels by the component of an applied radio-frequency (RF) field that is parallel to the NV symmetry axis (z axis). The transition frequency of this electron spin transition is 1.7 MHz in a static magnetic field of 28.9 G. In this system, the electron spin Rabi frequencies can reach tens of MHz even for moderate RF powers. Hence, this two-level system forms a very interesting platform for studying dynamics in the strong-driving regime. In the weak-driving regime, we observe clear sinusoidal Rabi oscillations of this two-level system. In the strong-driving regime, the dynamics become complex as the system oscillates with multiple frequencies and faster than the amplitude of the applied RF field.

All the experiments of this work have been performed using a home-built confocal microscope for optical excitation and detection of single NV centers and RF and microwave (MW) electronics for resonant excitation. The diamond crystal used has natural abundance of ^{13}C atoms and a nitrogen impurity concentration of <5 ppb.

II. SYSTEM AND HAMILTONIAN

The structure of an NV center coupled to a first-shell ^{13}C nuclear spin is illustrated in Fig. 1(a) along with its coordinate

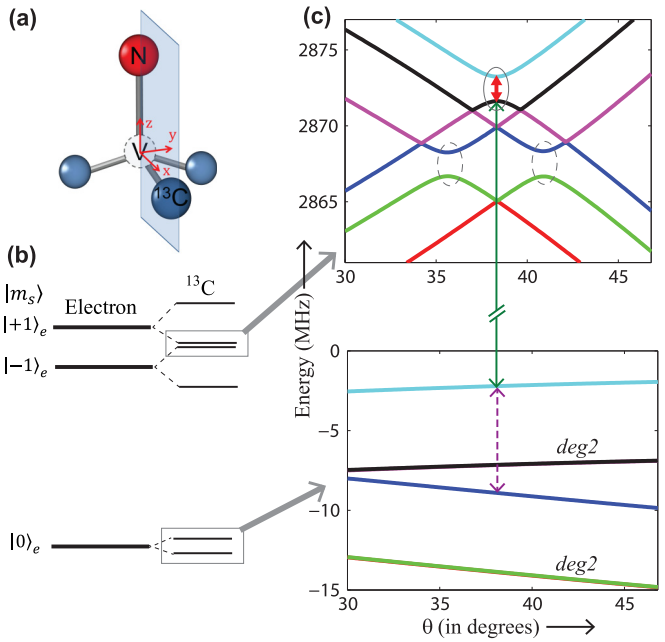

FIG. 1. (a) Structure of an NV center coupled to a first-shell ^{13}C nuclear spin. (b) Simplified energy level diagram of this system considering only the electron and the ^{13}C nuclear spins. (c) The energy levels marked by gray rectangles in (b) are plotted as functions of θ of a magnetic field of strength, $B = 28.9$ G, and $\phi = 0°$. Here, interactions due to the ^{14}N nuclear spin are also included. The energy levels labeled by *deg2* are nearly doubly degenerate. The transitions marked by thick red and thin green arrows are electron spin transitions, and the one marked by the dashed violet arrow is a ^{13}C nuclear spin transition.

system, which is defined as follows: The NV symmetry axis is defined as the z axis; the x axis is perpendicular to this axis and lies in the plane containing the nitrogen, the vacancy, and the ^{13}C atom; and the y axis is perpendicular to this plane. The total Hamiltonian of the system including the intrinsic ^{14}N nuclear spin of the center in this coordinate system can be written as

$$\mathcal{H} = DS_z^2 + \gamma_e \mathbf{B}\cdot\mathbf{S} + \gamma_{n1}\mathbf{B}\cdot\mathbf{I_1} + \gamma_{n2}\mathbf{B}\cdot\mathbf{I_2} + PI_{2z}^2 + \mathbf{S}\cdot\mathcal{A}_1\cdot\mathbf{I_1} + \mathbf{S}\cdot\mathcal{A}_2\cdot\mathbf{I_2}. \quad (1)$$

Here, $\mathbf{S}$, $\mathbf{I}_1$, and $\mathbf{I}_2$ represent spin angular momenta of the electron, ^{13}C and ^{14}N nuclei, respectively, and γ_e, γ_{n1}, and γ_{n2} the corresponding gyromagnetic ratios. $D = 2870.2$ MHz is the zero-field splitting, and $\mathbf{B} = B(\sin\theta\cos\phi,\ \sin\theta\sin\phi,\ \cos\theta)$ is the magnetic-field vector, where θ and ϕ represent its polar and azimuthal angles. $P = -4.95$ MHz [16] is the quadrupolar splitting of the ^{14}N nucleus, and $\mathcal{A}_1$ and $\mathcal{A}_2$ represent hyperfine tensors of the ^{13}C and ^{14}N nuclear spins, respectively, with the electron spin. The values for the hyperfine tensor components have been taken from previous work. For the ^{13}C nuclear spin, these are $\mathcal{A}_{1zz} = 128.9$, $\mathcal{A}_{1yy} = 128.4$, $\mathcal{A}_{1xx} = 189.3$, and $\mathcal{A}_{1xz} = 24.1$ MHz [17], and for the ^{14}N nuclear spin, these are $\mathcal{A}_{2zz} = -2.3$ MHz and $\sqrt{\mathcal{A}_{2xx}^2 + \mathcal{A}_{2yy}^2} = -2.6$ MHz [18–20]. All the other components of the hyperfine tensors are zero due to the symmetry of the system.

Now, we analyze the LACs that occur between the $m_s = -1$ and $+1$ spin states due to the strong nonsecular components of the Hamiltonian when the energy level splitting between them due to the Zeeman interaction of the electron spin is roughly equal to the energy splitting due to the ^{13}C hyperfine interaction: $2\gamma_e B\cos\theta$ is ≈127 MHz. Figure 1(b) shows a simplified energy level diagram, considering only the electron and ^{13}C nuclear spins. In this diagram, the energy levels relevant for the present work are marked with gray rectangles. These specific energy levels, after including the interaction with the ^{14}N nuclear spin, have been plotted as a function of θ of a static magnetic field of strength, $B = 28.9$ G, and $\phi = 0°$ in Fig. 1(c). For this magnetic-field strength, the LAC condition ($2\gamma_e B\cos\theta \approx 127$ MHz) corresponds to $\theta = 38.4°$. As can be seen from Fig. 1(c), there are several LAC points near $\theta = 38.4°$. Of these, the LACs relevant for the present work have been marked with gray ovals. These three LACs differ mainly with respect to the state of the ^{14}N nuclear spin. Here, we discuss specifically the LAC at $\theta = 38.4°$, which is marked with the solid gray oval and corresponds to $m_{I_2} = 0$. *The two energy levels shown in this gray oval represent the two-level system of which we study the strong-driving dynamics*. Away from the LAC, the electron spin states of these two levels are $m_s = +1$ and -1, and the transition between them is forbidden. At the LAC point, there is a strong mixing between the electron spin states, and the energy eigenstates become

$$|\psi_{1,2}\rangle \approx \left|\frac{|-1\rangle \pm |+1\rangle}{\sqrt{2}}, -\frac{1}{2}, 0\right\rangle,$$

where $-\frac{1}{2}$ and 0 represent spin states of the ^{13}C and ^{14}N nuclei, respectively. Consequently, a transition can be excited between these two levels by the z component (parallel to the NV axis) of the RF field as $|\langle\psi_1|S_z|\psi_2\rangle| \approx 1$.

The Hamiltonian of this two-level system can be written as

$$\mathcal{H}_{\rm TLS}(t) = \tfrac{1}{2}\omega_0\sigma_x + \omega_1\cos(2\pi\omega t)\sigma_z, \quad (2)$$

where, $\omega_0 = 1.7$ MHz is the transition frequency, and ω_1 and ω are the amplitude and frequency of the driving field, respectively. σ_x and σ_z are the Pauli spin matrices. In this system, ω_1 can have values that are more than an order of magnitude larger than ω_0 even for moderate RF powers, and hence it forms a very interesting system for experimental studies of strong-driving dynamics.

As discussed in Sec. I, the linearly oscillating driving field, $\cos(2\pi\omega t)\sigma_z$, can be written as a sum of co- $[\frac{1}{2}\cos(2\pi\omega t)\sigma_z - \frac{1}{2}\sin(2\pi\omega t)\sigma_y]$ and counter-rotating $[\frac{1}{2}\cos(2\pi\omega t)\sigma_z + \frac{1}{2}\sin(2\pi\omega t)\sigma_y]$ field components. In the weak-driving regime, i.e., $\omega_1 \ll \omega_0$, the rotating-wave approximation is valid and the counter-rotating field component can be neglected while the corotating field component drives Rabi oscillations of the system. These oscillations, damped by relaxation processes, were first observed in nuclear spins by Torrey [21]. The neglected counter-rotating field component was shown to shift the resonance frequency of the system by $\omega_1^2/4\omega_0$, which is known as Bloch-Siegert shift [22,23]. This shift, however, is very small when $\omega_1 \ll \omega_0$, and when ω_1 is of the order or greater than ω_0 (strong-driving regime), the approximations that are used to derive the shift themselves are not valid. In this strong-driving regime, the rotating-wave

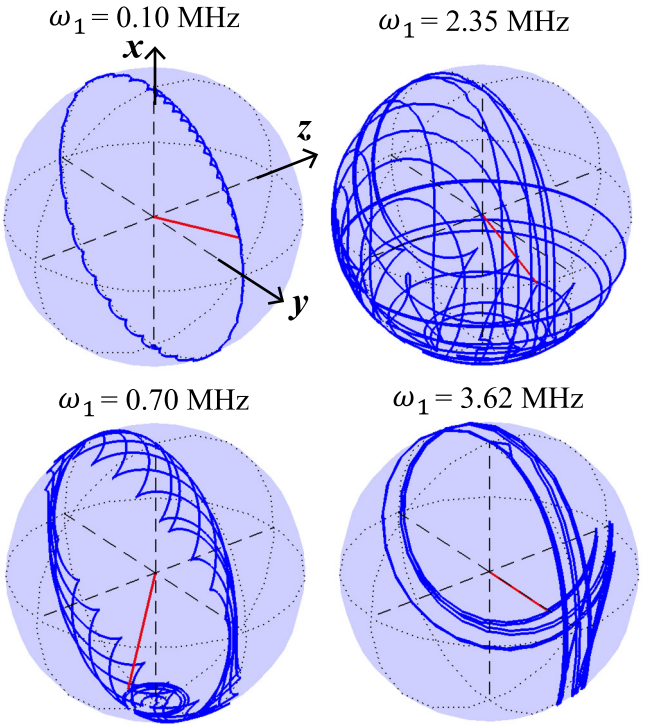

FIG. 2. Bloch sphere representation of the simulated on-resonance ($\omega = \omega_0 = 1.7$ MHz) rotating-frame dynamics of the system of Eq. (2) for different values of ω_1.

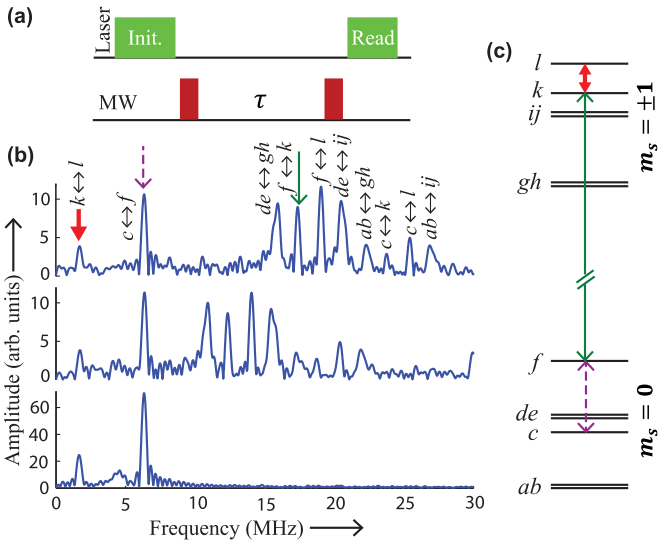

FIG. 3. (a) Pulse sequence used to measure Ramsey fringes. (b) Fourier transforms of Ramsey fringes, recorded at the LAC point $\theta = 38.4^\circ$ and $\phi = 0^\circ$. For the top and middle traces, the flip angle of the MW pulses was $\pi/2$ and the frequency detuning (ν_d) was 20 and 15 MHz, respectively. For the bottom trace, the flip angle was π. The spectral lines marked by thick red, thin green, and dotted violet arrows represent electron spin transitions of frequency 1.7 and 2873.9 MHz and a ^{13}C nuclear spin transition of frequency 6.4 MHz, respectively. (c) Corresponding energy level diagram at the LAC point. Energy levels labeled by two letters (e.g., *ab*) are nearly doubly degenerate.

approximation breaks down and both the co- and counter-rotating field components drive the system dynamics in a nontrivial way.

The Bloch sphere representation of the simulated on-resonance ($\omega = \omega_0$) dynamics of the above two-level system for different values of ω_1, in a frame rotating with the same frequency (ω) and direction of the corotating field component, are shown in Fig. 2. The system is initialized into the $|+x\rangle$ eigenstate of σ_x. When $\omega_1 = 0.10$ MHz ($\ll \omega_0 = 1.7$ MHz), where the rotating-wave approximation is valid, the system rotates on the surface of the sphere in the xy plane with a frequency ω_1. When $\omega_1 = 0.70$ MHz (comparable to ω_0), the system's dynamics deviate from the xy plane due to the counter-rotating field component. When $\omega_1 = 2.35$ MHz ($> \omega_0$), where the rotating-wave approximation is no longer valid, the spin trajectory occupies a large fraction of the surface of the sphere, and when $\omega_1 = 3.62$ MHz, the system does not flip to the $|-x\rangle$ state completely for any finite time t.

III. EXPERIMENTS

An experimental study of this two-level system requires precise orientation of the magnetic field with respect to the NV coordinate system. In this work, this was achieved by a permanent magnet placed at a fixed distance from the NV center and rotated around two orthogonal axes crossing at the NV center [17]. The magnetic field B was 28.9 G, oriented at $\theta = 38.4^\circ$ and $\phi = 0^\circ$, which corresponds to a LAC point [Fig. 1(c)]. The experimental electron spin resonance (ESR) spectra between the energy levels marked by gray rectangles in Fig. 1(b) at this magnetic field orientation are shown in Fig. 3(b). These were recorded as Fourier transforms of Ramsey fringes by using the pulse sequence shown in Fig. 3(a). All the spectral lines are labeled in comparison with the corresponding energy level diagram illustrated in Fig. 3(c). The frequency of the MW pulses was 2876.6 MHz. The phase of the second MW pulse ($-2\pi\nu_d\tau$) was varied with respect to that of the first pulse as a linear function of τ (delay between the pulses) such that an artificial detuning (ν_d) is introduced in the spectra. The top trace of these spectra was recorded with a frequency detuning (ν_d) of 20 MHz. In this spectrum, along with the electron spin transitions between the $m_s = 0$ and $m_s = \pm 1$ spin states (transitions in the range 15–30 MHz), two other transitions also appear. Of these, the transition that appears at 1.7 MHz (marked by the thick red arrow) is an electron spin transition between two levels of the $m_s = \pm 1$ manifolds. These two levels, which are shown inside the solid gray oval in Fig. 1(c), are the levels that we use to study the strong-driving dynamics. The other transition, which appears at 6.4 MHz (marked by the violet dashed arrow) is a ^{13}C nuclear spin transition of the $m_s = 0$ state.

These two transitions appear in the ESR spectrum indirectly as zero-quantum transitions [17]. For example, the transition between the two levels of the $m_s = \pm 1$ manifold can be excited by simultaneously driving the two transitions that connect these two levels with the same $m_s = 0$ spin sublevel (Raman excitation scheme). The zero-quantum nature of these transitions is clear by comparing the top trace of Fig. 3(b) with the middle trace of the same, which was recorded with a frequency detuning (ν_d) of 15 MHz. The transitions between the $m_s = 0$ and $m_s = \pm 1$ manifolds shift correspondingly by

FIG. 4. Pulse sequence for observing the dynamics of the two-level system.

5 MHz, whereas positions of the zero-quantum transitions do not change. The lower trace of Fig. 3(b) was recorded with the same pulse sequence of Fig. 3(a), but the flip angle of the MW pulses is π instead of $\pi/2$, which optimizes the signal from the zero-quantum transitions.

Now, we study the dynamics of the two-level system at the LAC [marked by solid gray oval in Fig. 1(c)]. These dynamics can be observed by using the pulse sequence shown in Fig. 4. Here, the first laser pulse polarizes the $m_s = 0$ spin state. The first MW π pulse applied at a frequency of 2873.9 MHz selectively inverts the transition marked by the solid green arrows in Figs. 1(c) and 3(b), which is a transition between the $m_s = 0$ and $m_s = \pm 1$ manifolds. This creates a population difference between the two levels of interest. Then an RF pulse of variable duration is applied on resonance ($\omega = \omega_0 = 1.7$ MHz) to drive the transition between the two levels. The corresponding dynamics are observed by applying another selective MW π pulse followed by the readout laser pulse, which reads the total population of the $m_s = 0$ state. The observed dynamics for different amplitudes (ω_1) of the RF pulse are shown in Fig. 5(a) (upper, blue curves). The values of ω_1 in the strong-driving regime are obtained by scaling the values measured in the weak-driving regime with the square root of the RF power. The corresponding dynamics simulated numerically using Eq. 2 are also shown in Fig. 5(a) (lower, red curves). The corresponding Fourier transforms are shown in Fig. 5(b). When the amplitude, ω_1, of the driving field is 0.23 MHz, which is small compared to the transition frequency, ω_0, of the system, the Rabi oscillations of the system are clearly sinusoidal. As we increase ω_1 to 1.6 MHz, which is close to $\omega_0 = 1.7$ MHz, the effects due to the counter-rotating field component become significant and the oscillations of the system deviate significantly from the simple sinusoidal behavior. When $\omega_1 > \omega_0$, the oscillations become strongly anharmonic as the effects due to the counter-rotating field component become more prominent. In this strong-driving regime, the system's dynamics contain frequency components that are significantly higher than the amplitude ω_1 of the field. This anharmonic and nonlinear behavior of the system can be seen from Fig. 5 when $\omega_1 = 2.35$ and 3.62 MHz: The system dynamics now includes multiple frequencies, some of which are higher than ω_1. The results of the numerical simulations, which are also shown in Fig. 5, are in good agreement with the experimental observations. However, there is some deviation between the experimental results and the simulated ones, in particular when $\omega_1 = 3.62$ MHz. This can be explained as follows.

In the strong-driving regime, the dynamics are very sensitive to the amplitude, phase, and shape of the RF pulse. In

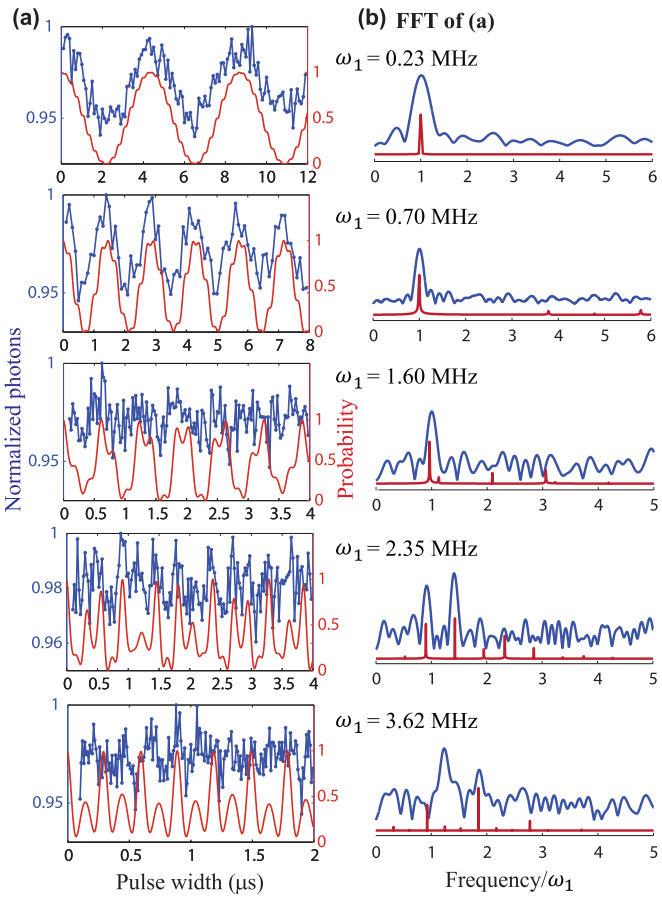

FIG. 5. Dynamics of the two-level system for increasing amplitudes, ω_1, of the driving field. (a) Dynamics as a function of the duration of the RF pulse. The upper, blue dots connected by solid lines are the experimental data and the lower red, solid curves are the corresponding simulated dynamics. (b) Fourier transforms of (a).

the present case, the deviations between the experiment and the simulation are mainly due to the effect of the phase of the RF pulse. Each data point of the experimental time-domain data was obtained by taking the average value over 200 000 repetitions of the pulse sequence shown in Fig. 4. The RF pulse of this pulse sequence was applied by chopping a continuous RF signal with an RF switch. This implies that the phase of this pulse is not the same in all the repetitions. This has no significant effect on the dynamics in the weak-driving regime. However, in the strong-driving regime, in particular when $\omega_1 > \omega_0$, this has significant effects. However, the phase of the RF pulse only alters the intensity pattern of the spectral peaks in the Fourier-transformed dynamics, not their positions (frequencies). This is explained in detail by using numerical simulations in the Appendix for the case $\omega_1 = 3.62$ MHz. This implies that the frequencies of the identifiable peaks of the experimental spectrum should match the frequencies of the peaks in the simulated one for any phase, but their amplitudes can be different. This can be observed in Fig. 5. When $\omega_1 = 3.62$ MHz, there is a strong peak in the experimental spectrum, roughly at frequency/$\omega_1 = 1.2$. At this position, there is also a peak in the simulated spectrum, but it is of very low intensity for the phase (0°) used in the simulation. This

experimental spectrum has a better match with the simulated one averaged over many different phases of the driving field (data shown in the Appendix).

IV. CONCLUSION

We studied, theoretically and experimentally, the anharmonic and nonlinear dynamics of a two-level system of a single spin driven in the strong-driving regime, where the rotating-wave approximation is not valid. Studying spin dynamics in this regime is interesting not only from the fundamental physics perspective but also to the quantum information processing because of the ultrafast quantum gates possible in this regime. The two-level system explored here will be useful to experimentally study strong-driving dynamics for very high ratios of driving field's amplitude to the transition frequency of the system. This system will also be useful as a good test bed to explore time-optimal pulse shapes in the strong-driving regime by using optimal control theory techniques [12,24–27].

ACKNOWLEDGMENTS

We acknowledge experimental assistance from Fabian Lehmann for the construction of the magnetic-field rotation setup. We thank Jingfu Zhang for useful discussions. This work was supported by the DFG through Grant No. Su 192/31-1.

APPENDIX

Effect of the phase of the driving field on the dynamics of the two-level system. We write the Hamiltonian of the two-level system as

$$\mathcal{H}_{\mathrm{TLS}}(t) = \tfrac{1}{2}\omega_0\sigma_x + \omega_1 \cos(2\pi\omega t + \varphi)\sigma_z.$$

This Hamiltonian is the same as in Eq. (2), except that the phase (φ) of the driving field is included here. In the weak-driving regime, this phase has no or negligible effect on the dynamics of the system. However, in the strong-driving regime, in particular when $\omega_1 > \omega_0$, this phase significantly affects the dynamics. In order to study this effect, we have numerically simulated the time-domain dynamics of the above two-level system for different values of φ when $\omega_0 = \omega = 1.7$ and $\omega_1 = 3.62$ MHz. The Fourier transforms of these time-domain dynamics are shown in Fig. 6. Figure 6(a) shows the spectra for three different values of φ. The intensity patterns of these spectra are significantly different from one another. However, note that it is only the intensities of the spectral peaks that change, but their positions (frequencies) remain the same. Figure 6(b) shows the Fourier transform of the average time-domain dynamics for 100 random values of φ between 0 and 180° in comparison with the experimental one for $\omega_1 = 3.62$ MHz. The match between the experiment and the simulation is better here than in Fig. 5.

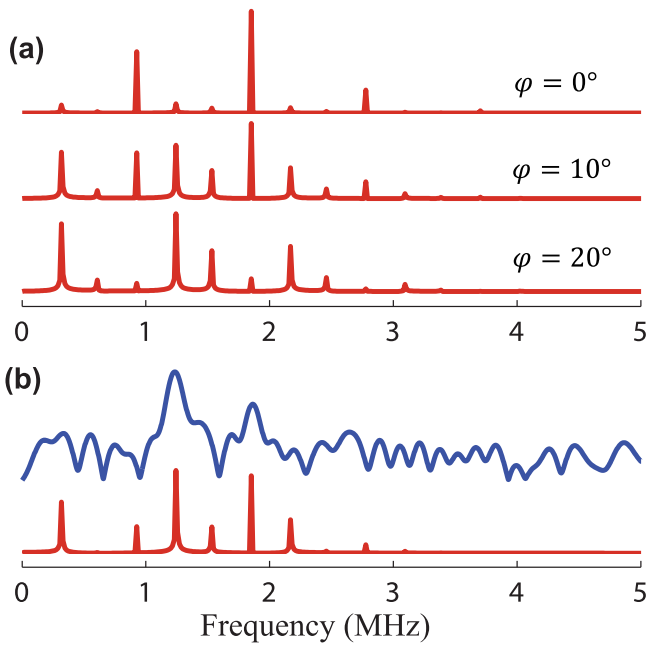

FIG. 6. (a) Fourier transforms of numerically simulated time-domain dynamics for three different values of φ when $\omega_0 = \omega = 1.7$ and $\omega_1 = 3.62$ MHz. (b) Fourier transform of these dynamics averaged over 100 random values of φ between 0 and 180° (lower spectrum) in comparison with the experimental one (upper spectrum).

[1] C. P. Slichter, *Principles of Magnetic Resonance* (Springer, New York, 1990).
[2] L. Allen and J. H. Eberly, *Optical Resonance and Two-Level atoms* (Dover, New York, 1987).
[3] M. A. Nielsen and I. L. Chuang, *Quantum Computation and Quantum Information* (Cambridge University Press, Cambridge, UK, 2000).
[4] F. Grossmann, T. Dittrich, P. Jung, and P. Hänggi, Phys. Rev. Lett. **67**, 516 (1991).
[5] J. K. Boyd, J. Math. Phys. **41**, 4330 (2000).
[6] S. Ashhab, J. R. Johansson, A. M. Zagoskin, and F. Nori, Phys. Rev. A **75**, 063414 (2007).
[7] L. Childress and J. McIntyre, Phys. Rev. A **82**, 033839 (2010).
[8] Y. Pomeau, B. Dorizzi, and B. Grammaticos, Phys. Rev. Lett. **56**, 681 (1986).
[9] J. Eidson and R. F. Fox, Phys. Rev. A **34**, 3288 (1986).
[10] G. D. Fuchs, V. V. Dobrovitski, D. M. Toyli, F. J. Heremans, and D. D. Awschalom, Science **326**, 1520 (2009).
[11] P. London, P. Balasubramanian, B. Naydenov, L. P. McGuinness, and F. Jelezko, Phys. Rev. A **90**, 012302 (2014).
[12] J. Scheuer, X. Kong, R. S. Said, J. Chen, A. Kurz, L. Marseglia, J. Du, P. R. Hemmer, S. Montangero, T. Calarco, B. Naydenov, and F. Jelezko, New J. Phys. **16**, 093022 (2014).
[13] C. Deng, J.-L. Orgiazzi, F. Shen, S. Ashhab, and A. Lupascu, Phys. Rev. Lett. **115**, 133601 (2015).
[14] A. Barfuss, J. Teissier, E. Neu, A. Nunnenkamp, and P. Maletinsky, Nat. Phys. **11**, 820 (2015).
[15] A. Laucht, S. Simmons, R. Kalra, G. Tosi, J. P. Dehollain, J. T. Muhonen, S. Freer, F. E. Hudson, K. M. Itoh, D. N. Jamieson,

J. C. McCallum, A. S. Dzurak, and A. Morello, Phys. Rev. B **94**, 161302 (2016).
[16] C. S. Shin, M. C. Butler, H.-J. Wang, C. E. Avalos, S. J. Seltzer, R.-B. Liu, A. Pines, and V. S. Bajaj, Phys. Rev. B **89**, 205202 (2014).
[17] K. R. K. Rao and D. Suter, Phys. Rev. B **94**, 060101 (2016).
[18] X.-F. He, N. B. Manson, and P. T. H. Fisk, Phys. Rev. B **47**, 8816 (1993).
[19] S. Felton, A. M. Edmonds, M. E. Newton, P. M. Martineau, D. Fisher, D. J. Twitchen, and J. M. Baker, Phys. Rev. B **79**, 075203 (2009).
[20] M. Chen, M. Hirose, and P. Cappellaro, Phys. Rev. B **92**, 020101 (2015).
[21] H. C. Torrey, Phys. Rev. **76**, 1059 (1949).
[22] F. Bloch and A. Siegert, Phys. Rev. **57**, 522 (1940).
[23] S. H. Autler and C. H. Townes, Phys. Rev. **100**, 703 (1955).
[24] N. Khaneja, R. Brockett, and S. J. Glaser, Phys. Rev. A **63**, 032308 (2001).
[25] U. Boscain and P. Mason, J. Math. Phys. **47**, 062101 (2006).
[26] P. Doria, T. Calarco, and S. Montangero, Phys. Rev. Lett. **106**, 190501 (2011).
[27] T. Caneva, T. Calarco, and S. Montangero, Phys. Rev. A **84**, 022326 (2011).